Experimental analysis of Taylor bubble behavior and mass transfer during lateral oscillation of a vertical milli-channel

Haghnegahdar, M.; Boden, S.; Hampel, U.;

Originally published:

May 2017

Chemical Engineering Journal 326(2017), 308-317

DOI: https://doi.org/10.1016/j.cej.2017.05.138

Perma-Link to Publication Repository of HZDR:

https://www.hzdr.de/publications/Publ-25746

Experimental analysis of Taylor bubble behavior and mass transfer during lateral oscillation of a vertical milli-channel

Mohammadreza Haghnegahdar, Stephan Boden, Uwe Hampel

PII: S1385-8947(17)30897-5
DOI: http://dx.doi.org/10.1016/j.cej.2017.05.138
Reference: CEJ 17037

To appear in: *Chemical Engineering Journal*

Received Date: 7 April 2017
Revised Date: 14 May 2017
Accepted Date: 22 May 2017

Please cite this article as: M. Haghnegahdar, S. Boden, U. Hampel, Experimental analysis of Taylor bubble behavior and mass transfer during lateral oscillation of a vertical milli-channel, *Chemical Engineering Journal* (2017), doi: http://dx.doi.org/10.1016/j.cej.2017.05.138

Experimental analysis of Taylor bubble behavior and mass transfer during lateral oscillation of a vertical milli-channel

Mohammadreza Haghnegahdar[a] (corresponding author)

[a] Institute of Fluid Dynamics, Helmholtz-Zentrum Dresden - Rossendorf, Bautzner Landstr. 400, 01328 Dresden, Germany. Phone: +49 351 260 3767, Fax: +49 351 260 2383, Email: m.haghnegahdar@hzdr.de

Stephan Boden[a]

[a] AREVA Endowed Chair of Imaging Techniques in Energy and Process Engineering, Technische Universität Dresden, 01062 Dresden, Germany. Email: s.boden@hzdr.de

Uwe Hampel[a,b]

[a] Institute of Fluid Dynamics, Helmholtz-Zentrum Dresden - Rossendorf, Bautzner Landstr. 400, 01328 Dresden, Germany.

[b] AREVA Endowed Chair of Imaging Techniques in Energy and Process Engineering, Technische Universität Dresden, 01062 Dresden, Germany.

Experimental analysis of Taylor bubble behavior and mass transfer during lateral oscillation of a vertical milli-channel

Abstract

In this paper, we report on an experimental study on the influence of low-frequency horizontal vibration of a vertical millimeter-size channel with Taylor bubbles. We investigated the motion, shape and dissolution rate of individual elongated Taylor bubbles of air and CO_2, which were freely rising in stationary water. Bubble size and dissolution rate were determined from microfocus X-ray radiographs. From the shrinking rate we calculated the liquid-side mass transfer coefficient. The rise velocity of bubbles and surface wave motion were analyzed using a videometric technique. The comparison of the results for the stationary and the oscillating channel showed that mechanical vibration of the channel is able to enhance the mass transfer coefficient from gas to the liquid phase by 80% to 186%, depending on the frequency and amplitude of vibration. It was found that channel oscillation causes the increase of free rise velocity of bubbles which is mainly attributed to the development of propelling interfacial waves and increase of liquid film flow rate. Furthermore, analyzing the surface wave motion of bubbles revealed that the enlargement of contact area between the phases and the increased mixing enhances the mass transfer additionally up to 30% compared to non-agitated bubbles of similar Peclet number.

1 Introduction

Multi-phase chemical reactors with micro- and millimetre-size channel structures are considered as a promising alternative to conventional multiphase reactors, such as bubble columns and fixed bed reactors which are widely used for gas absorption, catalytic hydrogenation, biochemical conversions, direct fluorination and others. The main advantages of small channel multiphase reactors are creation of a large volumetric interfacial area, low-pressure drop, and ease of scale-up. However, because the

governing flow regime in such reactors is laminar, the liquid-side mass transfer coefficient (k_L) between the phases is lower than for turbulent flow in e.g. bubble columns or stirred tank reactors [1]. To enhance the individual mass transfer coefficient, one of the most recently considered methods is applying structural vibration or sound fields to agitate the fluidic phases. Such approaches were demonstrated for many conventional multi-phase contactors and proved their ability to intensify the mass transport processes [1],[2]. In the following, the most relevant studies on the application of ultrasound and vibration in gas-liquid contacting systems will be shortly reviewed.

One of the first investigations on the effect of axial vibration on bubble-bed gas absorbers has been carried out by Harbaum and Houghton [3]. They demonstrated a noticeable enhancement in mass transfer performance in the frequency range 20 Hz to 200 Hz. Jaeger and Kurzweg [4] investigated the longitudinal dispersion in oscillatory pipe flow of binary gas mixtures at high axial oscillation frequencies. It was shown that the magnitude of the dispersion coefficient is directly related to the product of the frequency and the square of oscillation amplitude. For elongated Taylor bubbles, Brannock and Kubie [5] were the first to investigate the influence of vibration on the free rise velocity of bubbles [6]. They measured the rise velocity of long bubbles while exposing the vertical pipes to an axial sinusoidal motion. It was found that an acceleration of up to 10 m/s^2 had no considerable influence on the bubble shapes while for acceleration up to 15 m/s^2 the bubbles started to distort. The bubble nose became more elongated and its curvature increased. The results indicate that the bubble rise velocity increases as the acceleration decreases. For a horizontal motion of vertical channels, Kubie [7] performed a similar study and investigated the rise velocity of elongated bubbles. It was shown that the mean bubble velocity is a function of the pipe diameter, the relative acceleration and the amplitude of the sinusoidal motion and increases as the relative acceleration increases. He also compared the increasing trend of the bubble rise velocity in horizontal direction with the decreasing rise velocity for vertical channel vibration and showed that the reason for this difference is the direction and magnitude of resulting acceleration acting on the bubbles.

Ellenberger and Krishna [8],[9] discussed the application of low-frequency vertical vibrations to the liquid phase of an air–water bubble column. They mounted a vibration exciter at the bottom of the bubble column which transfers the vibration to the liquid phase by means of a piston. They showed

that vibration causes to produce considerably smaller bubbles at the nozzle. Also, it was shown that application of vibrations causes enhancement of mass transfer coefficient and gas hold up by a factor of two or more [10]. Furthermore, the results showed that application of vertical oscillation has the potential of enhancing the contacting of phases in fluid-fluid dispersions [11],[12]. Dillon et al. [13] investigated the pressure drop of two-phase flow in a narrow horizontal annular test section with an inner diameter of 7.93 mm. The influence of lateral mechanical oscillation of the test section on two-phase pressure drop was investigated, with vibration amplitudes up to 0.2 mm and frequencies in the range 5 Hz to 400 Hz. The results showed a negligible influence of the vibration, which was within the experimental uncertainty limits. The impact of low-frequency vertical vibrations on the hydrodynamics and mass transfer characteristics of monolith loop reactors was studied by Vandu et al. [14] and compared with conventional internal airlift reactor and bubble column configurations. The results showed that imposing oscillation has the effect of significantly improving the ratio of volumetric mass transfer coefficient to the gas hold up for all considered reactor configurations. For monoliths, it was moreover found that vibrations additionally improve the gas–liquid distribution across the channels.

Hashmi et al. [15] reviewed current knowledge about the underlying physics of oscillating bubbles in micro-sized contactors. They critically discussed state of the art on the application of oscillation in microfluidic devices. They also highlighted the benefits and the challenges of using vibrating bubbles and argued that these investigations would be revolutionary to the progress of next-generation Lab-on-Chip systems. Madani et al. [6] considered the rise of a Taylor bubble in a vertical vibrating channel. The experiments were done for two different pipe diameters and with fluids of different viscosities and restricted to high Reynolds numbers to study the inertial effects. The results showed that for low acceleration the average velocity decreases with the relative acceleration of oscillation. Also, it was shown that, beyond a critical relative acceleration, the mean bubble velocity rises and the increase of fluctuating velocity slow down. Fernandez Rivas et al. [16] reviewed concepts of micro-sono-reactors and discussed the latest progres and future directions. They discussed that micro-sono-reactors are capable of handling small reaction volumes in a reproducible and efficient system, which the main parameters of the system such as frequency, amplitude, acoustic power, and sonication times can be

accurately adjusted. Moreover, it was argued that processes including the micro-sono-reactors are easily scalable and enable flow recirculation.

Polezhaev et al. [17] found a significant increasing evaporation rate in a tube in which the gas/liquid interface axially oscillates and reported a tenfold increase of the apparent diffusive coefficient. The dependency of the enhancing effect on the tube diameter, the frequency and the amplitude of the liquid oscillations was investigated and the parametric dependence of the apparent diffusive coefficient was correlated via the associated dimensionless Péclet number. Yao [2] gave an overview over the recent investigations on the application of power ultrasound to adsorbent regeneration, food drying, air dehumidification, water treatment and others. They concluded that although the ultrasonic treatment may cause degradation of especially biological process constituents, it can significantly help to decrease the food processing time and reduce the drying temperature. Recently, Dong et al. [18] used ultrasonic oscillation to intensify the gas-liquid mass-transfer in micro-reactors. They applied severe surface wave vibration on the bubbles and found that for slug bubbles confined in a smaller microchannel, surface wave oscillations require more ultrasound energy to excite due to the confinement effect. It was proven that the volumetric mass-transfer coefficient increased by 3 to 20 times under oscillation. Furthermore, it was shown that for gas-liquid flow hydrodynamics, oscillation disrupts the bubble formation process and alters the initial bubble size and pressure drop [1].

As it was briefly summarized, oscillation/vibration of transferring phases is one of a promising and efficient approach to intensify transport processes. However, on one hand, most of the investigations are focused on the micro-sized reactors and little attention has been paid to the millimeter-sized channels such as monolithic reactors. On the other hand, most reported studies were devoted to axial or vertical oscillation of channels, which has some drawbacks for process itself, such as stronger axial back mixing and decreasing the rise velocity of the gas phase.

In the work reported in this paper, the hydrodynamics and mass transfer behavior of a single Taylor bubble in quiescent water, whose motion is governed by the channel walls, was investigated inside of a laterally vibrated vertical channel of 6 mm inner diameter using the combination of microfocus X-ray radiography technique and optical videometry. The amplitude, A, and frequency, f, of vibration

are in the range of 0 to 0.7 mm and 0 to 44 Hz, respectively. The liquid-side mass transfer coefficient was determined from microfocus X-ray images. This technique was qualified to disclose the three-dimensional shape of Taylor bubbles in millimeter-sized channels [19] and enabled the acquisition of a series of high-resolution radiographic images of Taylor bubbles. The processed images which give volume and length of the bubble with high accuracy as a function of time were used to evaluate the liquid-side mass transfer coefficient using the mass conservation equation.

The X-ray method was chosen for mass transport study since it is not dependent on the refractive index of the channel. Experimental investigations aiming at the disclosure of bubble shapes, slug and bubble lengths and wall film thickness where mainly performed with optical techniques. Examples are given in Yao et al. [20], Zhu et al. [21], Kolb et al. [22], Thulasidas et al. [23] and Fries at al. [24]. The optical methods used so far for capillary flow visualization and measurement have in common, that optical access is required (transparent liquids and channels with smooth walls) and full 3D bubble shape is hard to be measured. X-ray imaging represents a promising approach to continue this research towards arbitrary channel cross-sections, intransparent phases and components, rough and intransparent channel walls as well as oscillating channels.

2 Material and methods

2.1 Experimental setup

The experimental setup is schematically shown in Fig. 1a while the imaging instrumentation is presented in more detail in Fig. 1b. The setup consists of the 300 mm long round glass tube (observation section), lower and upper liquid reservoirs, a gas injection system, temperature gauges, an X-ray source, a flat panel X-ray detector, a liquid flow controller system, CO_2 bottles and liquid flow metering system. The inner diameter of the tube was measured by Vernier calipers and was 6 mm. The uncertainty in measurement was determined as ±0.05 mm. The tube is made of borosilicate glass with a wall thickness of about 2 mm. Degassed deionized water with electrical conductivity <0.5 µS/cm, surface tension 72.70×10^{-3} N/m and pH 7 was fed into an open-air overhead reservoir. The

reservoir was covered by a plastic head to prevent intrusion of dust particles. The temperature was fixed at about 293±1 K. A level indicator was installed in the upper reservoir to obtain the hydraulic static pressure.

The glass tube is placed between the X-ray source and a two-dimensional flat panel X-ray image detector. It is fixed between two horizontal arms which are connected on the vibrator. The arms transform the horizontal sinusoidal motion of vibrator to the capillary. In this study the liquid is quiescent and the single Taylor bubbles are freely rising and there is no downward liquid flow to fix the bubble in front of the X-ray source. The passing of single bubbles takes about 2 seconds depending on the size of the bubbles. A Taylor bubble is generated by the injection of some finite amount of gas into the liquid through an axially aligned metallic needle inside the tube and upstream the observation section [25]. The amount of gas injected into the liquid is controlled by a remotely operated fast acting solenoid valve. Gas is provided either by a gas cylinder (laboratory CO_2 bottle, 99.99% purity, Air Liquide GmbH) or a pressured air. Various bubble equivalent diameters (1 mm – 25 mm) can be produced by changing the duty cycle parameters of the gas injection valve.

Fig. 1b shows the top view of actuator and imaging instrument. It comprises of an X-ray source, a flat panel X-ray detector, a high-resolution camera, a LED light source, the mechanical vibrator, and laser confocal displacement meter (LCDM). The X-ray source is a microfocus X-ray tube (X-RAY WorX XWT-190-TC) equipped with a tungsten high energy transmission target. The maximum tube voltage is 150 kV at a maximum target power of 25 W. In this study a tube voltage of 135 kV and a tube current of 40 µA was used to not exceed 5 W target power and to achieve the smallest focal spot size and thus highest spatial resolution. The X-ray parameters were held fixed during all experiments. The X-ray detector is a two-dimensional flat panel X-ray detector (Perkin Elmer XRD 0822 AP3 IND) equipped with a high efficiency/high-resolution cesium iodine (CsI) scintillation screen. The resolution of the detector is 1024 x 1024 px at a pixel size of 200 µm x 200 µm. Thus the detector covers an area of 20 cm x 20 cm. An integration time of 100 ms per image was chosen for the radioscopic measurements. The Taylor bubble was radioscopically monitored at an exposure time of 100 ms and a frame rate of 10 Hz. The mechanical vibrator (Otto Schön, 11075) is connected to the

amplifier which is able to vibrate the vertical channel in the horizontal (lateral) direction in a continuous frequency range of 3 Hz to 80 kHz and amplitude up to 7.00 mm. However, in this study the imposed amplitude and frequency of vibration were in the range of 0 – 0.7 mm and 0 – 44 Hz, respectively. Due to the mechanical limitations of the experimental setup, it was not possible to impose broader amplitudes for high frequencies. The amplifier is controlled by a wave form generator (Agilent 33250A). The signal of the generator is transferred to the amplifier and then to the vibrator. The strength of the signal is adjusted by both the amplifier and generator.

The Camera is a CCD video camera (AVT Pike, F-100B) which continuously monitored the bubble's position in an axial range of 30 mm. The camera is connected to the PC via a digital interface and is controlled using AVT smart view software. The camera is fixed on an adaptable support which enables positioning of the camera to adjust the field of view. The recorded images of the bubble oscillation were processed using MATLAB. The laser confocal displacement meter (Keyence, LT9030M) is a high accuracy surface scanner with the resolution of 0.01 µm which is used to adjust and measure of the amplitude of channel vibration.

2.1.1 Procedure

The protocol of each set of experiments is as follows. Before starting the experiments a high countercurrent flow rate was adjusted and a large number of bubbles were injected into the liquid to flush the injection needle and pipes and to ensure that they were filled with the injection gas only. At the beginning of the experiments a number of reference images were acquired showing the liquid filled tube only. The desired value of frequency for channel vibration was set for the vibrator. The value of the amplitude of oscillation was measured by the LCDM and controlled by changing the output power of the wave form generator. Then, a bubble was injected into the liquid. As soon as the ascending bubble reached the field of view, the CCD camera recording was started. Synchronously, we scanned the bubble by X-ray imaging during the dissolution process of bubble.

Fig. 1

2.2 X-ray image processing

2.2.1 Bubble size measurement

The description of X-ray image processing and measurement calibration used in this study have been presented in detail elsewhere [26]. Thus only a brief description will be given here. The X-ray radioscopic data comes as intensity images. An intensity image is further denoted as a two-dimensional matrix $\boldsymbol{I}$ of dimensions $N_i \times N_j$ and with values $I_{i,j}$ for each pixel. Each pixel represents the intensity along an X-ray defined by the spatial positions of the focal X-ray spot of the source and the detector pixel. For each of those rays we can compute an image of linear extinction values

$$\boldsymbol{E} = -log\left(\frac{\boldsymbol{I}}{\boldsymbol{I_0}}\right) \quad (1)$$

with $\boldsymbol{I}_0$ denoting the ray intensity for a reference state, that is, no object in the field of view. The extinction value is a linear measure of ray attenuation caused by objects in the ray path.

Geometric calibration of the X-ray imaging system is best achieved by visualization of an object with known spatial dimensions. The two maxima of the horizontal extinction profile [26], which was vertically averaged over 600 detector rows, give the positions of the projected inner glass wall of the tube. The cylindricity of the circular glass channel was checked using the microfocus X-ray computed tomography and the diameter was found to vary by 0.5%, and the inner diameter of the channel was determined to be 5.96 ± 0.03 mm. With the known inner tube diameter all X-ray images were geometrically calibrated to an effective pixel spacing of 29.0 µm ± 0.5%.

In order to quantify the bubble length and volume, an extinction image $\boldsymbol{E}_b$ showing the Taylor bubble only was computed by subtraction

$$\boldsymbol{E}_b = \boldsymbol{E}_g - \boldsymbol{E}_{ref}, \quad (2)$$

as exemplarily given in Fig. 2a. In this equation, $\boldsymbol{E}_g$ is the radiographic extinction image of a bubble in the liquid-filled tube and $\boldsymbol{E}_{ref}$ is the radiographic extinction image of the liquid-filled tube only.

The extinction images $\boldsymbol{E}_b$ were noisy due to the short exposure times; thus extraction of geometrical details was prone to errors. Therefore, a set of dedicated calibration measurements was conducted

[26]. Non-dissolving air bubbles were injected into the liquid and were held at a fixed vertical position by application of a countercurrent liquid flow. Since the reference bubbles were not shrinking, the computation of average extinction images $\overline{\boldsymbol{E}}_b$ by superposition of a set of at least 128 single time exposures was possible (Fig. 2b). Such image exhibited a signal to noise ratio sufficient for bubble shape analysis. The projected 2D bubble interface was extracted (Fig. 2c), and volume of the reference bubbles were computed by construction of a solid of revolution of the interfacial profile. The relative error in the measurement of the projected interfacial curve was estimated to be ± 1 px, thus resulting in an uncertainty of the volume computation which is lower than 2.5% for bubble sizes considered in this study [26]. Then, the reference bubbles' volume, V_b, was correlated to the measured integral extinction $\sum_{ij} \overline{\boldsymbol{E}}_b$ in the form of linear equations [19],[26],

$$V_b = k_V \sum_{ij} \overline{\boldsymbol{E}}_b \qquad (3).$$

Therein, k_V is calibration constant which was found by linear regression of the data of nine calibration experiments covering three different bubble sizes. The bubble length L_b is computed as the distance between the maximum and minimum z-position of the extracted projected bubble interface along the channel axis.

Fig. 2

Image averaging, however, is not possible during studies of mass transfer, since the bubble shape is continuously changing. Fig. 3 shows X-ray radiographs of dissolving (CO_2) bubbles in oscillating channel. As it can be seen, bubble rising and oscillation of channel in stagnant liquid cause undesired motion blur. The size of each X-ray radiographs was 15 mm x 30 mm. This size comes from a compromise to have the maximum field of view to trace the bubble on one hand, and to have the maximum spatial resolution and minimum signal to nose ratio on the other hand. During the mass transfer study the change in the volume of bubble was different and depending upon the amplitude and frequency of vibration, it varied between 4% and 14% of initial volume of bubble. As a result, only the

integral extinction $\sum_{ij} \boldsymbol{E}_b$ of non-averaged X-ray images (Fig. 2a) was measured as a function of time, and correlations equivalent to equation 3 was used to infer instantaneous bubble volume and their dynamics; thereby utilizing beforehand measured calibration constants [27].

Due to the finite exposure time, channel oscillation causes periodically changing blur of the X-ray projections, which in turn causes periodical variations in calculated integral attenuation $\sum_{ij} \boldsymbol{E}_b$ when using a static reference, $\boldsymbol{E}_{ref}$. Amplitude and phase of that periodically changing offset were estimated using fast Fourier transformation (FFT) analysis and the fluctuating integral attenuation was corrected accordingly.

The uncertainty in measured $\sum_{ij} \boldsymbol{E}_b$ was less than 2%, the uncertainty in measurement of V_b is the same due to equation (3) which is included in uncertainty calculation of mass transfer coefficient.

Fig. 3

2.3 Measurement and adjustment of the vibration amplitude

The oscillation induces a horizontal motion of the vertical channel axis and as it was mentioned, the frequency and amplitude of oscillation were controlled by wave form generator. But, the resulting amplitude of the motion cannot be deduced from the wave form generator signals and therefore we measured and set its value using the LCDM at the beginning of each experiment. However, due to injection and movement of bubble, in some cases, the oscillation amplitude of channel was slightly affected. Therefore, the videoscopic observation data from CCD camera with effective pixel resolution of 108 µm was used to double check the data. Fig. 4 shows the measured channel vibration amplitudes from the videography data.

Fig. 4

3 Results and discussion

3.1 Bubble shape and rise velocity

Fig. 5 exemplarily shows a non-dissolving Taylor bubble as it rises in the oscillating channel within one full period of oscillation. As Hashmi et al. [15] discussed, bubbles could be considered as a soft membrane which is able to oscillate under the action of excitation. Depending upon the frequency and amplitude of the external vibration, the reaction of the bubble can be linear or non-linear. As it can be seen, the horizontal channel motion forces the liquid via its momentum to the backside of the channel (with respect to motion direction) and thus pushes the bubble tip in the direction of motion. As a result, the liquid film thickness increases at the backside of the tube; which leads to downward movement of additional amount of liquid along the Taylor bubble side.

Furthermore, the channel oscillation causes waves on the surface of bubble which travel along the bubble axis. As it can be seen in Fig. 5, on one hand, the surface wave axial velocity is mainly related to liquid velocity in the film. On the other hand, the waves on the surface of the bubble are not symmetric. This behavior was also reported by Kubie [7] in laterally oscillating vertical pipes and also by Madani et al. [6] for axial vibration of vertical tubes. For the later case Madani et al. [6] conjectured that the non-axisymmetric surface wave motion leads to a higher downward liquid flowrate and also an increase of bubble rise velocity.

Fig. 5

The free rise velocity of bubbles (U_b) in the stagnant liquid in the channel was precisely measured utilizing the CCD video camera which monitored the front tip of bubbles. The position of the bubble's front tip was tracked over an axial range of 30 mm at a frame rate of 188.2 frames per second and an effective pixel resolution of 108 µm. Depending on the rise velocity of bubbles, 180 to 950 images were analyzed and tracked to measure the rise velocity of bubble. This way we obtained the instantaneous bubble front tip free rise velocity. We cross-compared these data to the ones obtained

from the X-ray radiographic images and found that the difference between the measured values by two methods is about 2%.

Fig. 6 shows the measured rise velocity of a freely rising non-dissolving (air) Taylor bubble in the circular channel as a function of channel oscillation frequency. We studied bubbles between L_b = 20 mm and 22 mm and d_{eq}/D of 1.5 to 1.6, where L_b is bubble length, D channel hydraulic diameter, and d_{eq} sphere-volume equivalent bubble diameter. The maximum uncertainty in measured bubble rise velocity is estimated to be 3%.

As it can be seen, for non-oscillating channel the Taylor bubbles rises at 6.9 mm/s. An increasing amplitude and frequency of the horizontal channel motion leads to increase of the bubble rise velocity. Moreover, the amplitude of vibration has a considerable influence on the rise velocity of the bubbles. For example, at 26 Hz a change of amplitude from 0.3 mm to 0.7 mm causes an increase of bubble velocity from 10.11 mm/s to 28.95 mm/s.

Furthermore, as it can be seen, the data show some intensifying effect at certain frequencies. At these frequencies the bubble vibration and bubble rise velocity reach their maximum value. This behavior is consistent with the observation of the Ellenberger et al. [9] for gas holdup of bubble columns. They showed that vertical vibration of bubble columns show some enhancing effect at specific frequencies where the gas holdup is maxima. In our system, our observations revealed that this intensifying effect is more pronounced at higher amplitude and is dependent upon the parameters of mechanical system.

Fig. 6

3.2 Interfacial waves

The horizontal channel oscillation induces surface waves on the left and right-hand side of the Taylor bubble (left and right with respect to the observers point of view), which travel downward on the bubble interface. The travel velocity is assumed to be constant, which seems to be true at least for the center part of the Taylor bubble away from the front and rear bubble cap. Fig. 7 presents the surface

wave travel velocity. The values of the surface wave travel velocity plotted in this figure are averages of at least three measurements. The error bars indicate one standard deviation about the mean points.

The surface wave travel velocity shows a similar behavior as the bubble rise velocity. It increases with increasing amplitude and frequency of channel motion. In detail, the maximum and minimum of both the bubble velocity and bubble surface wave velocity are the same which means that the increase and decrease of bubble rise velocity are corresponding with the variation of bubble surface wave velocity. Moreover, it should be noted that for large amplitude oscillations of the channel, at the frequencies where the rise velocity is maximum, a slight vertical oscillation of channels was observed which can affect the motion of oscillating bubbles. Furthermore, videometric observation reveals that with increasing of oscillation amplitude, the bubble surface oscillation increases progressively, which starts from volume pulsation to the small surface waves and then to chaotic surface distortion which is in accordance with data reported by Dong et al. [1] in horizontal microchannels.

Fig. 7

The videoscopic data of non-dissolving bubbles (Fig. 5) show periodic occurrence of bubble surface waves. The surface wave occurrence frequency was measured and is shown in Fig. 8. As it can be seen, the surface waves occur at exactly the same frequency as the horizontal channel oscillation (one new wave per horizontal motion period) and are independent of the oscillation amplitude. This behavior is in contrast with the observation of Dong et al. [1] in microchannels which indicated that the bubble surface waves oscillate periodically at half the driving frequency, which is a key feature of the Faraday wave.

Fig. 8

3.3 Mass transfer coefficient

3.3.1 Mass transfer calculation

For a CO_2 bubble absorbing into water the resistance to mass transfer in the gas phase is negligible with respect to the resistance in the liquid phase under the prevailing conditions [28]. Therefore the rate of mass transfer is proportional to the difference of interface and bulk concentration of the liquid phase

$$-\frac{dn}{dt} = k_L A_b (C^* - C). \quad (4)$$

In this equation n is the total moles of gas phase (CO_2) inside the bubble, t the time, C^* the concentration of gas at the interface, A_b the surface area of bubble based on the bubble sphere-volume equivalent diameter (d_{eq}), and C the concentration of gas in the liquid bulk. Due to the channel oscillation, the bubble surface was very wavy and calculation of bubble interfacial area is uncertain. As a result, bubble surface area was reported based on the calculations of an equivalent bubble diameter. The bubble equivalent diameter defines as the diameter of a sphere with the volume equals to the volume of the bubble. This method which is widely used for Taylor bubble flow [29],[30],[31] is appropriate for reproducibility of the measured mass transfer coefficient with knowing the initial bubble volume.

Assuming the equilibrium at the interface by Henry's law and because $C \ll C^*$, we have

$$\frac{dn}{dt} = -k_L A_b \frac{C_L P y}{H - P y}, \quad (5)$$

where H is Henry's constant, C_L the water concentration, y the mole fraction of CO_2 in the gas phase and P the pressure inside the bubble calculated by

$$P = P_{atm} + \rho_L g h. \quad (6)$$

Here P_{atm} is atmospheric pressure, h the distance from the liquid surface in the upper reservoir to the center of the bubble. The contribution of Laplace pressure can be neglected (lower that 0.03%) because the bubble size is relatively large. Moreover, variation of bubble pressure due to the rising of bubble (Δh=30 mm) is less than 0.4%, therefore P could be assumed constant during the experiments.

Due to atmospheric pressure of the bubble, the ideal gas law can be applied for the gas phase, therefore we can replace *dn/dt* in terms of V_b (volume of bubble) as

$$\frac{\mathrm{d}n}{\mathrm{d}t} = \frac{P}{RT}\frac{dV_b}{dt}, \qquad (7)$$

where *R* is universal gas constant and *T* the gas temperature.

Hosoda et al. [29] have shown that for the first ten seconds from the injection of the bubbles the CO_2 composition inside the bubbles can be considered as unity. However, in our experiments to calculate the k_L, we only considered initial first second of CO_2 dissolution and as a result, the counter diffusion of air from liquid to bubble is negligible. Therefore by assuming *y* as unity and by combining Eq. 6 and 7 we have

$$k_L = -\frac{1}{A_b RT}\frac{H-P}{C_L}\frac{dV_b}{dt}. \qquad (8)$$

The mass transfer was calculated by applying a difference scheme to determine dV_b/dt. The values of constant parameters are shown in Table. 1.

Table. 1 The values of constant parameters

Parameter	**Value (298 K)**
Density (ρ)	998.2 (kg/m^3)
Henry constant for CO_2 (H)	189 (MPa)
Water concentration (C_L)	55.4 (kmol/m^3)
Molecular diffusivity for CO_2 in water (D_c)	1.6×10^{-9} (m^2/s)

3.3.2 Mass transfer coefficient

We carried out the experiments to measure the influence of vibration frequency and amplitude on the mass transfer rate. The liquid-side mass transfer coefficients, k_L, according to Eq. (8) for individual rising dissolving Taylor bubbles in stagnant liquid are shown in Fig. 9. For dissolving bubble experiments (CO_2 bubbles) the injected (initial) bubble size was set to L_b=19 mm to 22 mm and d_{eq}/D=1.5 to 1.6. The values of the mass transfer coefficient plotted in this figure are averages of at least three measurements. The error bars indicate one standard deviation about the mean points.

As it can be seen, oscillation causes an increase of the mass transfer coefficient in comparison with the non-oscillation case (single point at f=0 Hz). At constant vibration amplitude, an increase of frequency causes also an increase of mass transfer coefficient. The rise of k_L is not even and has some fluctuations. For vibration with an amplitude of 0.7 mm, at frequencies larger than 30 Hz due to very large shape oscillations of bubbles and high bubble rise velocity, the number of data to calculate the mass transfer coefficient was not enough. Therefore, k_L could not be measured and reported. However, the trend shows a clear rising behavior of k_L. Furthermore, increase of oscillation amplitude leads to an increase of the mass transfer rate, which is more pronounced for higher amplitudes. For example for a vibration amplitude of 0.3 mm, the liquid-side mass transfer coefficient increases at maximum by 79.9%, while the increase is 186.1% for a vibration amplitude of 0.5 mm.

Fig. 9

For a better understanding of the behavior of dissolving bubbles the free rise velocity of CO_2 bubbles was measured and is given in Fig. 10. The measurement conditions and procedure were the same as air bubbles. The maximum uncertainty in measured bubble rise velocity is estimated to be 3%. As it can be seen, an increase of vibration frequency and amplitude causes faster motion of rising bubbles, which is in accordance with the non-dissolving bubbles (Fig. 6). However, there are some differences in the trend of rise velocity between CO_2 and air bubbles. The local maximum points are more pronounced for non-dissolving bubbles compared to the CO_2 bubbles. The reason could be attributed to the multipart behavior of dissolving bubbles. On one hand, CO_2 bubbles are dissolving and their front tip is shrinking which means their front tip is descending and at the same time whole bubble is rising. On the other hand, because of dissolution of bubble, the bubble volume is decreasing which also affects hydrodynamics of the bubble and consequently the free rise velocity of bubbles which causes some differences in trend of dissolving and non-dissolving bubble rise velocity.

Moreover, comparison of Fig. 9 and Fig. 10 shows that there is a fairly good consistency between the values of mass transfer coefficient and bubble rise velocities. For example in the range of our

experiment for a vibration amplitude of 0.3 mm, the maximum bubble rise velocity occurs at frequencies 32 Hz to 34 Hz and k_L also has a maximum at this frequency.

On the other hand, as it was shown in Fig. 6 and Fig. 7, for any vibration amplitude considered in this study, the trend and the peak values of bubble rise velocities are corresponding to the trend and peak values of bubble surface waves, which means that the rise velocity and surface wave velocity are directly related to each other. Therefore, in case of CO_2 bubbles where there is a fairly good agreement between the values of mass transfer coefficient and bubble rise velocities, it can be concluded that the increase and decrease of mass transfer coefficient of rising bubbles as a function of vibration amplitude and frequency is a function of bubble surface wave velocity.

Fig. 10

Furthermore, as it can be seen in Fig. 5, the bubble surface wave oscillation directly influences the hydrodynamics of the liquid film and therewith the gas–liquid interface in the falling liquid film region around the bubble and causes an increase of mixing in this region. As it is known, the flow regime in this region is laminar and mass transfer is performed due to diffusion mechanism between the layers. Therefore, vibration of channel causes the reduction of the liquid-side mass transfer resistance between the streamlines and consequently leads to the enlargement of mass transfer rate. On the other hand, bubble surface waves generated by channel oscillation cause the increase of interfacial area between the bubbles and liquid phase which is another mechanism for enhancement of mass transfer.

For overall comparison of dissolution rate of bubbles in oscillating and non-oscillating channel, the mass transfer rate of oscillating bubbles were calculated in the form of non-dimensional Sherwood number, *Sh*, and Peclet number, *Pe*. Sherwood number, which represents the ratio of convectional mass transfer to the diffusional mass transfer, is a common way to report the mass transfer coefficient of dissolving bubbles and defines as

$$Sh = \frac{k_L d_{eq}}{D_c}, \quad (9)$$

$$Pe = \frac{U_b d_{eq}}{D_c}, \quad (10)$$

where D_c is the gas molecular diffusion coefficient.

Since, to calculate the mass transfer from elongated bubble, it is required to know the product of $k_L A_b$, we reported the data in the form of modified Sherwood number, Sh^*, which is defined as:

$$Sh^* = \frac{k_L A_b}{D_c D} \quad (11)$$

where D is the channel hydraulic diameter. The Sherwood number data are shown in Fig. 11. The prediction of the correlation developed by Haghnegahdar et al. [26] is also presented. This correlation is developed for the mass transfer of elongated bubbles in water in non-oscillating millimeter sized-channels with a hydraulic diameter ranging from 6.0 mm to 8.0 mm and is defined as:

$$Sh^* = \left(23.003(d_{eq}/D)^2 - 38.623(d_{eq}/D) + 23.591\right)Pe^{0.5} \quad for\ 0.8 < (d_{eq}/D) < 1.6\,. \quad (12)$$

As it can be seen in Fig. 11, for low amplitude vibration (A=0.3 mm) and also for channel oscillations with high amplitude but low frequencies, the experimental data fits to our previously derived correlation for non-oscillating bubbles. It should be noted, however, that the non-oscillating bubbles were held stationary in a downward flow of liquid while the agitated bubbles propel themselves through stagnant liquid. At about $Pe^{0.5}$=280 higher amplitude and frequencies of the oscillation do not only increase the bubble velocity (Peclet number) but also the mass transfer beyond the prediction of the correlation for non-oscillating bubbles. This increase in mass transfer is gained from the deformation turbulence induced by the shaking.

To sum up, the intensification of mass transfer with increase of amplitude/frequency of vibration is primarily attributed to the increase of the bubble surface wave oscillation that causes an enlargement of contact area between the phases and a reduction of mass transfer resistance in the liquid-side boundary layer [14]. Nonetheless, understanding the exact mechanism of mass transfer enhancement and obtaining a fundamental model require a more detailed analysis in the future.

Fig. 11

4 Conclusion

The motion, shape and dissolution rate of individual elongated Taylor bubbles of air and CO_2 in the water was studied in a millimeter-size channel to investigate the effect of low-frequency horizontal vibration of the channel. The bubbles were freely rising in stationary liquid and the liquid-side mass transfer coefficient was determined from microfocus X-ray images. The acquired X-ray images of the bubbles were analyzed with respect to volume, surface area and length of the bubble and were utilized to obtain the mass transfer coefficient. The rise velocity and surface wave motion of bubbles were analyzed via videometric observation with a CCD camera. The comparison of the results for the stationary and oscillating channel showed that

- mechanical vibration of the channel is able to enhance the liquid-side mass transfer coefficient between the gas and liquid phases in millimeter-sized channels from 80% to 186%;
- the mass transfer rate positively correlates with frequency and amplitude of oscillation, which is more pronounced for higher amplitude;
- channel oscillation causes an enlargement of free rise velocity of bubbles, which is mainly attributed to development of bubble surface waves;
- the intensification of mass transfer with increase of amplitude/frequency of vibration is mainly attributed to the increase of the bubble surface wave oscillation that causes an enlargement of contact area between the phases and also a reduction of mass transfer resistance in the liquid-side boundary layer.

Acknowledgement

This work is funded by the German Research Foundation (DFG), priority program “Transport processes at fluidic interfaces”, SPP 1506. The authors thankfully acknowledge the financial support.

Notation

A_b	bubble surface area based on the bubble sphere-volume equivalent diameter (d_{eq})
a	specific interfacial area
C^*	concentration of gas at interface
C	concentration of gas at the liquid bulk
C_L	water concentration
d	bubble diameter
d_{eq}	sphere-volume equivalent bubble diameter
D	channel hydraulic diameter
D_c	gas molecular diffusion coefficient
E	radiographic extinction image
f	channel vibration frequency
g	acceleration due to gravity
h	distance from the liquid surface
H	Henry's constant
I	X-ray intensity
k_L	liquid-side mass transfer coefficient
k_v	calibration function
L_b	bubble length
n	total moles of gas inside the bubble
P	pressure inside of the bubble
P_{atm}	atmospheric pressure
Pe	Peclet number
R	universal gas constant
Sh	Sherwood number
t	time
T	bubble temperature
U_b	bubble free rise velocity

V_b	bubble volume
y	mole fraction of CO_2 inside of gas phase
z	axial direction
ρ	liquid density

References

[1] Z. Dong, C. Yao, Y. Zhang, G. Chen, Q. Yuan, J. Xu, Hydrodynamics and Mass Transfer of Oscillating Gas-Liquid Flow in Ultrasonic Microreactors, AIChE J. 62 (2016) 1294–1307.

[2] Y. Yao, Enhanceinent of mass transfer by ultrasound Application to adsorbent regeneration and food drying dehydration, Ultrason. Sonochem. 31 (2016) 512–531.

[3] K.L. Harbaum, G. Houghton, Letters to the Editors Letters to the Editors, Chem. Eng. Sci. 13 (1960) 90–92.

[4] M.J. Jaeger, U.H. Kurzweg, Determination of the longitudinal dispersion coefficient in flows subjected to high-frequency oscillations, Phys. Fluids. 26 (1983) 1380–1382.

[5] D. Brannock, J. Kubie, Velocity Of Long Bubbles In Oscillating Vertical Pipes, Int. J. Multiph. Flow. 22 (1996) 1031–1034.

[6] S. Madani, O. Caballina, M. Souhar, Unsteady dynamics of Taylor bubble rising in vertical oscillating tubes, Int. J. Multiph. Flow. 35 (2009) 363–375.

[7] J. Kubie, Velocity of long bubbles in horizontally oscillating vertical pipes, Int. J. Multiph. Flow. 26 (2000) 339–349.

[8] R. Krishna, J. Ellenberger, Improving gas-liquid contacting in bubble columns by vibration excitement, Int. J. Multiph. Flow. 28 (2002) 1223–1234.

[9] J. Ellenberger, R. Krishna, Improving mass transfer in gas – liquid dispersions by vibration excitement, Chem. Eng. Sci. 57 (2002) 4809–4815.

[10] R. Krishna, J. Ellenberger, Influence of low-frequency vibrations on bubble and drop sizes formed at a single orifice, Chem. Eng. Process. 42 (2003) 15–21.

[11] J. Ellenberger, J.M. Van Baten, R. Krishna, Intensification of bubble columns by vibration excitement, Catal. Today. 79–80 (2003) 181–188.

[12] J. Ellenberger, R. Krishna, Shaken, not stirred, bubble column reactors: Enhancement of mass transfer by vibration excitement, Chem. Eng. Sci. 58 (2003) 705–710.

[13] C.M. Dillon, S.M. Ghiaasiaan, S.I. Abdel-Khalik, S.M. Jeter, D.L. Sadowski, Two-phase

pressure drop in a horizontal thin annulus: Effects of channel vibration and wall gas injection, Exp. Therm. Fluid Sci. 30 (2005) 67–78.

[14] C.O. Vandu, J. Ellenberger, R. Krishna, Hydrodynamics and mass, transfer in an upflow monolith loop reactor, Chem. Eng. Process. Process Intensif. 44 (2005) 363–374.

[15] A. Hashmi, G. Yu, M. Reilly-Collette, G. Heiman, J. Xu, Oscillating bubbles: a versatile tool for lab on a chip applications., Lab Chip. 12 (2012) 4216–4227.

[16] D. Fernandez Rivas, P. Cintas, H.J.G.E. Gardeniers, Merging microfluidics and sonochemistry: towards greener and more efficient micro-sono-reactors, Chem. Commun. 48 (2012) 10935.

[17] D. Polezhaev, P. Duru, F. Plouraboué, Enhanced evaporation from an oscillating liquid in a capillary tube, Int. J. Heat Mass Transf. 95 (2016) 288–295.

[18] Z. Dong, C. Yao, X. Zhang, J. Xu, G. Chen, Y. Zhao, et al., A high-power ultrasonic microreactor and its application in gas–liquid mass transfer intensification, Lab Chip. 15 (2015) 1145–1152.

[19] S. Boden, M. Haghnegahdar, U. Hampel, Measurement of Taylor bubble shape in square channel by microfocus X-ray computed tomography for investigation of mass transfer, Flow Meas. Instrum. 53 (2016) 49–55.

[20] C. Yao, Z. Dong, Y. Zhao, C. Guangwen, An online method to measure mass transfer of slug flow in a microchannel, Chem. Eng. Sci. 112 (2014) 15–24.

[21] C. Zhu, C. Li, X. Gao, Y. Ma, D. Liu, Taylor flow and mass transfer of CO2 chemical absorption into MEA aqueous solutions in a T-junction microchannel, Int. J. Heat Mass Transf. . 73 (2014) 492–499.

[22] W.B. Kolb, R.L. Cerro, Coating the inside of a capillary of square cross section , Chem. Eng. Sci. . 46 (1991) 2181–2195.

[23] T.C. Thulasidas, M.A. Abraham, R.L. Cerro, Bubble-train flow in capillaries of circular and square cross section , Chem. Eng. Sci. . 50 (1995) 183–199.

[24] D.M. Fries, P.R. von Rohr, Impact of inlet design on mass transfer in gas-liquid rectangular microchannels, Microfluid. Nanofluidics. 6 (2009) 27–35.

[25] M. Haghnegahdar, S. Boden, U. Hampel, Mass transfer measurement in a square milli-channel and comparison with results from a circular channel, Int. J. Heat Mass Transf. 101 (2016) 251–260.

[26] M. Haghnegahdar, S. Boden, U. Hampel, Investigation of mass transfer in milli-channels using high-resolution microfocus X-ray imaging, Int. J. Heat Mass Transf. 93 (2015) 653–664.

[27] M. Haghnegahdar, S. Boden, U. Hampel, Investigation of surfactant effect on the bubble shape

and mass transfer in a milli-channel using high-resolution microfocus X-ray imaging, Int. J. Multiph. Flow. 87 (2016) 184–196.

[28] M. Muradoglu, G. Tryggvason, A front-tracking method for computation of interfacial flows with soluble surfactants, J. Comput. Phys. 227 (2008) 2238–2262.

[29] S. Hosoda, S. Abe, S. Hosokawa, A. Tomiyama, Mass transfer from a bubble in a vertical pipe, Int. J. Heat Mass Transf. 69 (2014) 215–222.

[30] K. Tsuchiya, H. Mikasa, T. Saito, Absorption dynamics of CO2 bubbles in a pressurized liquid flowing downward and its simulation in seawater, Chem. Eng. Sci. . 52 (1997) 4119–4126.

[31] K. Niranjan, M.A. Hashim, A.B. Pandit, J.F. Davidson, Liquid-phase controlled mass transfer from a gas slug, Chem. Eng. Sci. . 43 (1988) 1247–1252.

Fig. 1 Schematic drawing of the experimental setup:

a) Hydraulic circuit with observation section (1), microfocus X-ray source (2), flat panel X-ray image detector (3), vibrator (4), remotely controlled motorized needle valve (5), upper reservoir (6), lower reservoir (7), video camera (8), gas injection line (9), fast solenoid valve (10), gas cylinder (11),

b) Top view of special instrumentation and actuators: LCDM (12), Mechanical vibrator (13), CCD camera (14), LED light source for illumination (15)

Fig. 2 (a) Extinction image of a dissolving Taylor bubble as it passes the X-ray detector (raw data). (b) Averaged image of the 'calibration bubble', whose position was held fixed in front of the X-ray detector by countercurrent liquid flow. (c) Extracted bubble interface projection (solid line)

Fig. 3 X-ray radiographs of dissolving (CO_2) bubbles in oscillating channel (f = 40 Hz)

Fig. 4 Measured channel vibration amplitude using the videoscopic data from CCD camera

Fig. 5 An air Taylor bubble (not dissolving in the liquid) as it rises in the oscillating channel within one full period of oscillation (f = 12 Hz). The vertical position of the surface wave crest on the Taylor bubble's left and right hand side is indicated by the dashed and continuous line. The relative horizontal position of the tube is indicated by the marker at the bottom of each image

Fig. 6 Measured rise velocity of a freely rising non-dissolving Taylor bubble in circular channel as a function of channel oscillation frequency and amplitude

Fig. 7 Surface wave travel velocity of rising bubbles

Fig. 8 Surface wave occurrence frequency of rising bubbles

Fig. 9 Measured mass transfer coefficient for oscillating bubbles with initial size $1.5 < d_{eq}/D_c < 1.6$

Fig. 10 Free rise velocity of dissolving bubbles

Fig. 11 The experimental data for oscillating channels in the form of modified Sherwood number accompanying with predicted data by the correlation proposed by Haghnegahdar et al. [20]

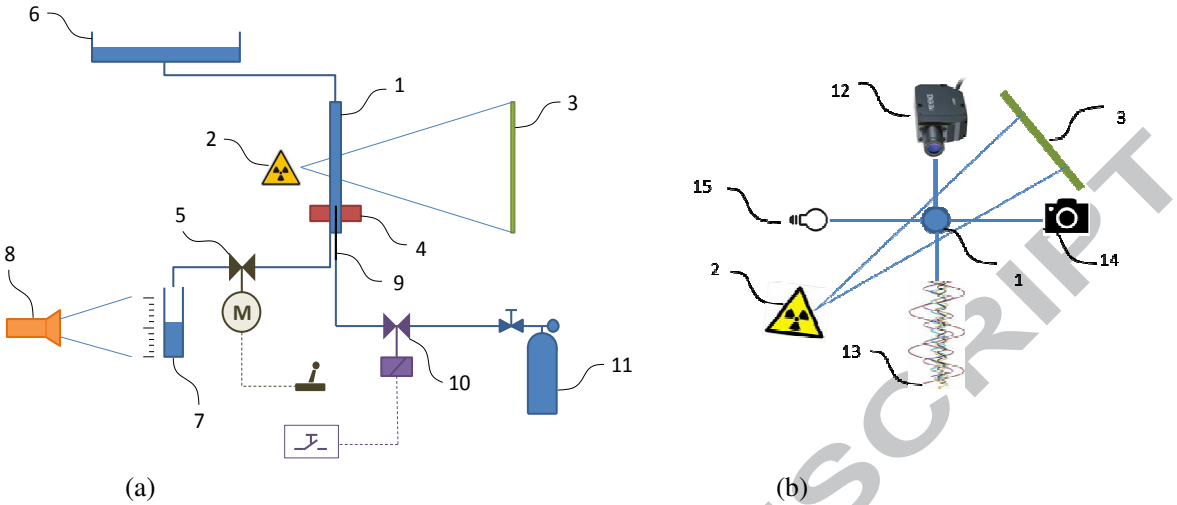

(a) (b)

Fig. 1

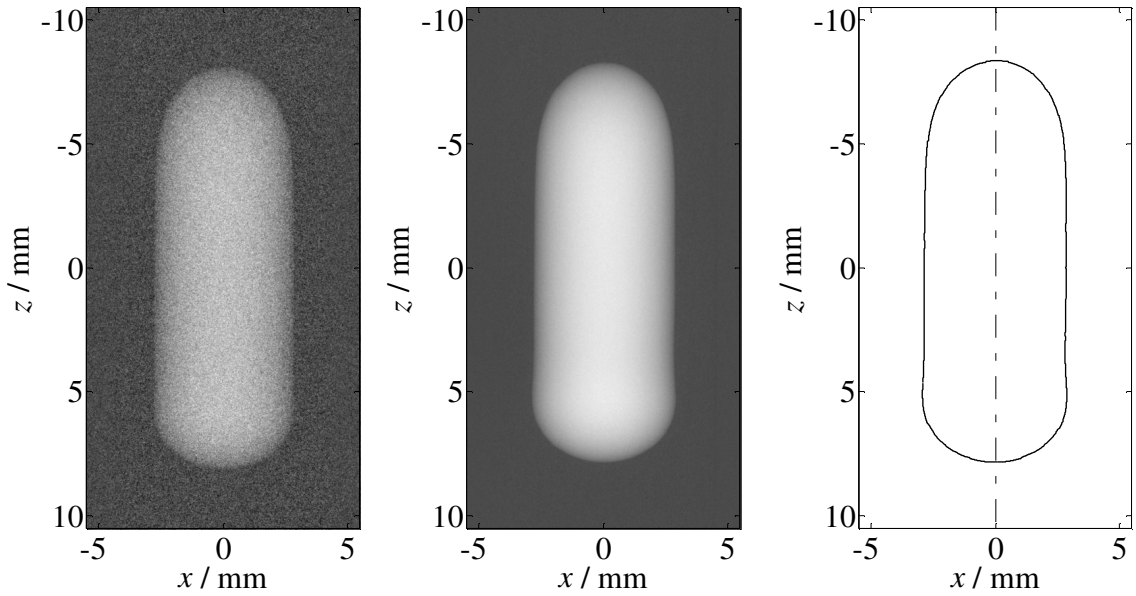

(a) (b) (c)

Fig. 2

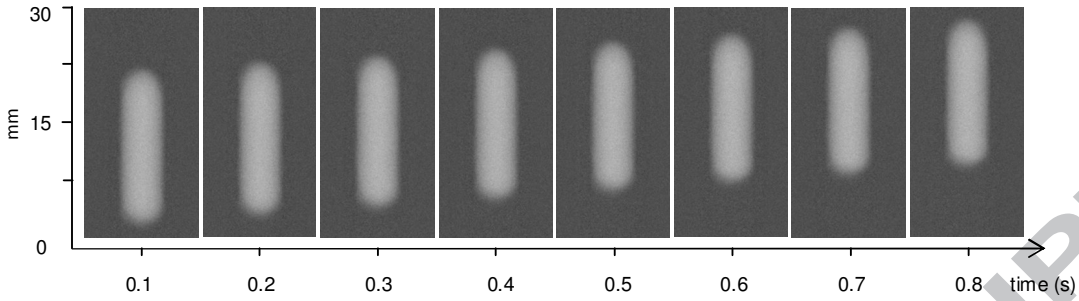

Fig. 3

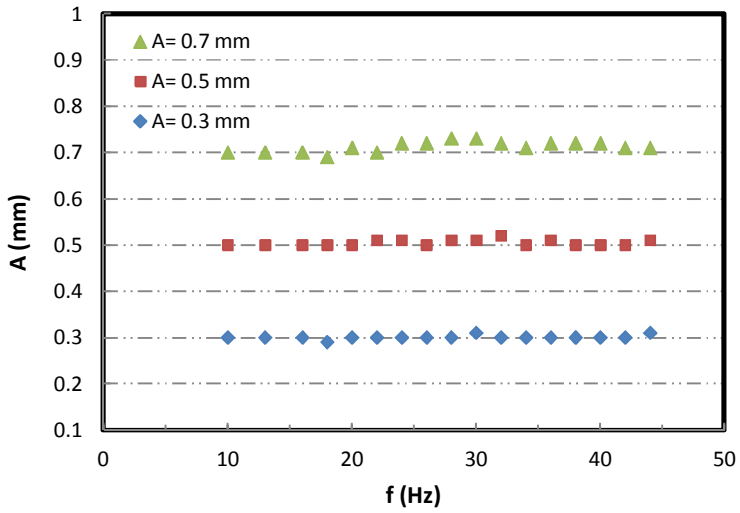

Fig. 4

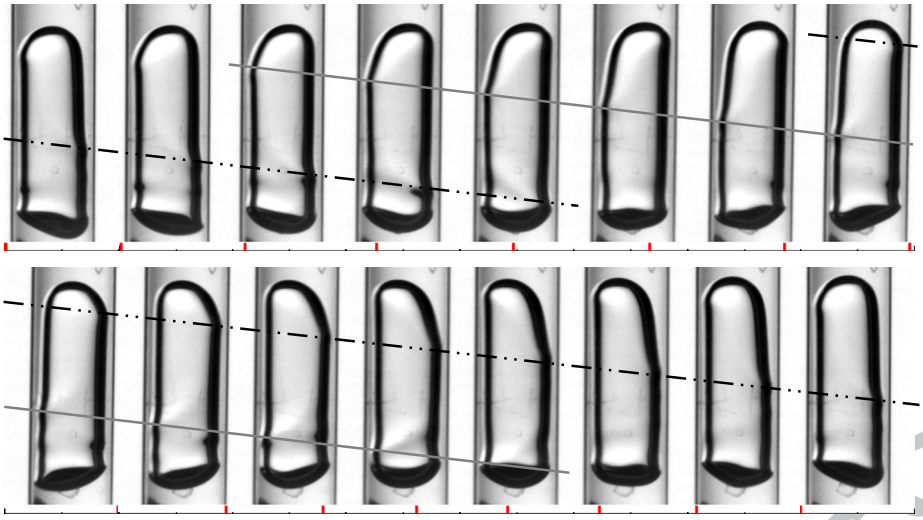

Fig. 5

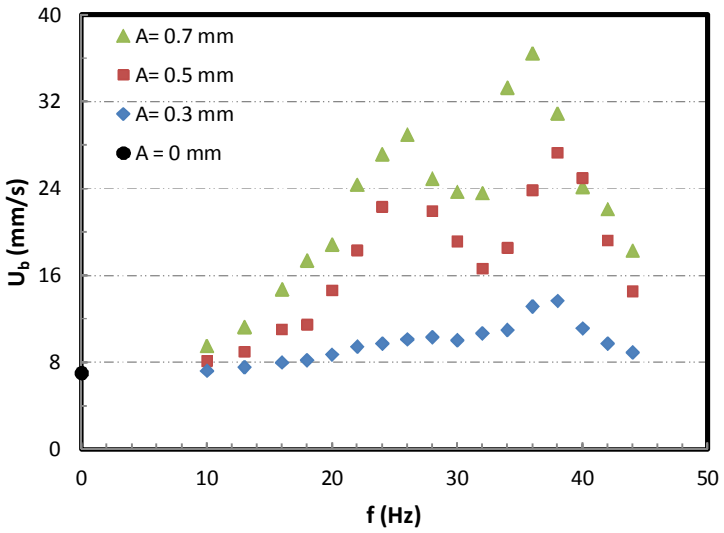

Fig. 6

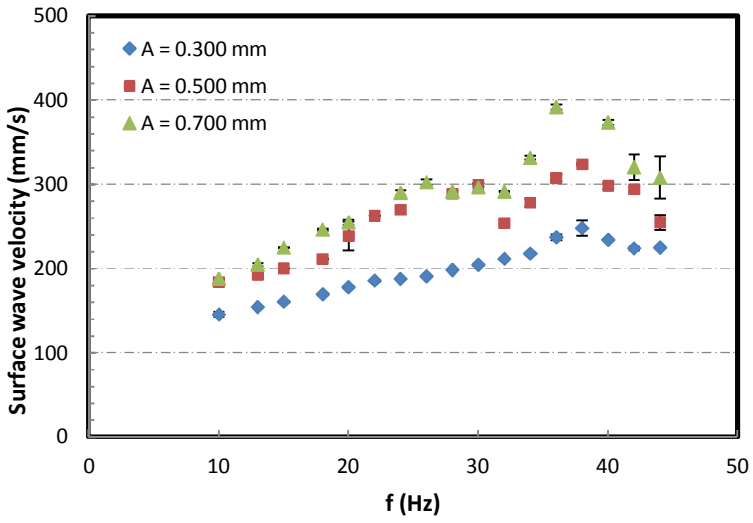

Fig. 7

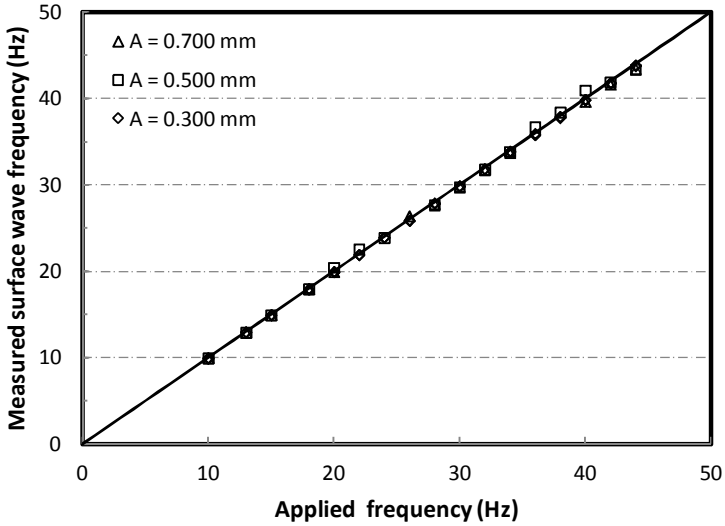

Fig. 8

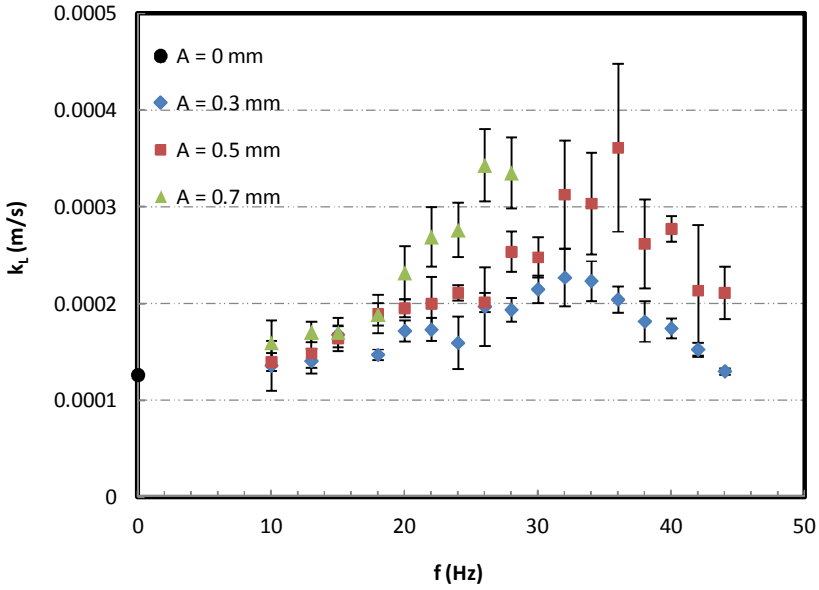

Fig. 9

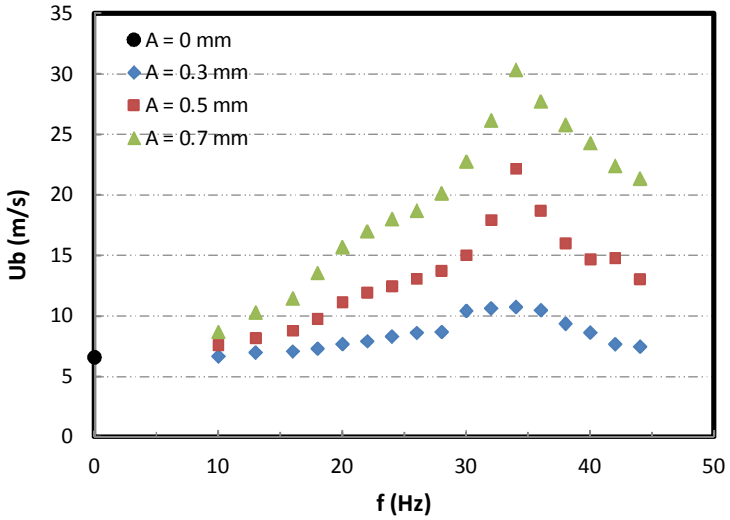

Fig. 10

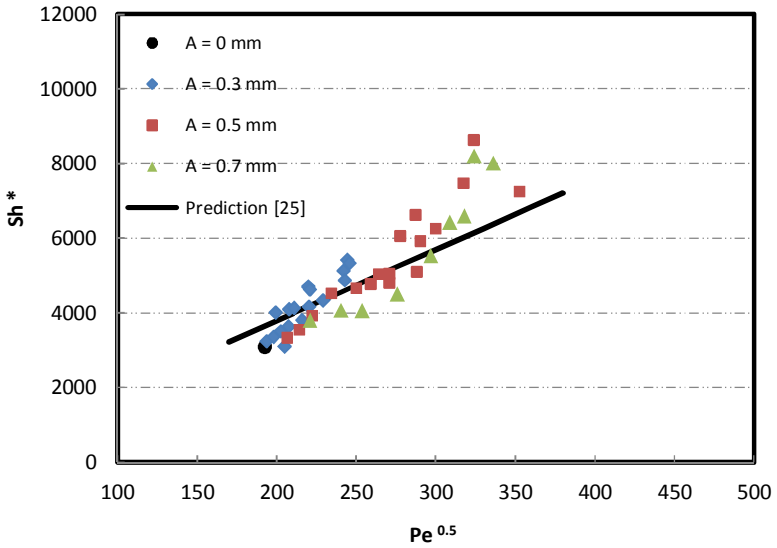

Fig. 11

Highlights

- X-ray imaging was used to study the effect of channel vibration on the mass transfer of bubbles.
- The mass transfer rate positively correlates with frequency and amplitude of channel vibration.
- Channel oscillation causes an enlargement of free rise velocity of bubbles.
- Channel oscillation intensifies the surface wave motion of bubbles and causes enhancement of mass transfer.